

## RESEARCH ARTICLE

# Investigation into the improved axial compressibility of a spinning non-ideal gas

Yi-Wen Zhang<sup>1</sup>, Shi-Long Su<sup>1</sup>, Shu-Bin Xie<sup>1</sup>, Wei-Min Zhou<sup>2</sup>, Hao Liu<sup>1,3,\*</sup><sup>1</sup>Department of Applied Physics, School of Physics and Electronics, Hunan University, Changsha 410082, China<sup>2</sup>Science and Technology on Plasma Physics Laboratory, Laser Fusion Research Center, China Academy of Engineering Physics, Mianyang 621900, China<sup>3</sup>HEDPS, Center for Applied Physics and Technology, Peking University, Beijing 100086, China

Corresponding author. E-mail: \*haoliu@hnu.edu.cn

Received January 10, 2020; accepted February 15, 2020

Using theoretical analysis and numerical calculation method, the axial adiabatic compression of a spinning non-ideal gas in a cylinder with a smooth surface is investigated. We show that the axial pressure of a spinning gas will gradually become lower than that of a stationary gas during continuous compression, even though the initial axial pressure of the spinning gas is larger than that of the stationary gas at the same initial temperature and average density. This phenomenon indicates that the axial compressibility of gas is improved in a rotating system. In addition, the effect of different forms of virial coefficient  $B(T)$  on pressure and temperature changes in spinning and stationary gases are investigated. Research on the axial compressibility of spinning non-ideal gas can provide useful references for fields that require high compression of gases, such as laser fusion, laboratory astrophysics, and Z-pinch experiments.

**Keywords** compressibility, spinning system, non-ideal gas, virial EOS

## 1 Introduction

The high compression of matter is of great importance in many science and engineering fields, such as inertial confinement fusion [1, 2], high energy density physics [3], high-pressure science [4], Z-pinch experiments [5, 6], and laboratory astrophysics [7]. The method for compressing materials is divided mainly into dynamic impact compression and quasi-static compression. In inertial confinement fusion, an ultra-strong laser-driven shock wave is used to compress fusion fuel to 1 000 times solid density.

The thermodynamic quantities of a substance, such as temperature  $T$ , pressure  $p$ , and internal energy  $U$  change with the change in density  $\rho$  during the compression process. These changes are not only related to the equation of state (EOS) of the material being compressed, but also to the specific compression method selected. Taking shock compression [8–10] as an example, for a uniform gas system in the same initial state, the gas density can be compressed by a factor of three by applying a strong shock, or the same compression ratio can be achieved by sequentially loading two or more weaker shock waves. At the same final  $\rho$  value, the  $T$  and  $p$  values obtained from multiple shocks will be significantly lower than those produced by a single shock. The quasi-static compression process can be regarded as a continuous compression of numerous weak shock waves; therefore, the increase in  $T$  and  $p$

values is the smallest of all the adiabatic methods.

Can we find another compression path in which the pressure increase is even slower than in a quasi-static compression? Previous theoretical work, conducted by Geyko *et al.* [11], studied the compression process of a spinning ideal gas and found that the  $p$ -increase of the ideal gas in a spinning system during quasi-static adiabatic compression was lower than that in a stationary system, indicating the improved axial compressibility of spinning gas. The reason for this result is that the energy of external  $p\mathrm{d}V$  work can be stored in the rotational kinetic energy  $E_r$  during compression, and the increase in  $T$  for spinning gas is less than that of stationary gas.

The axial compression process of a spinning non-ideal gas with an EOS of virial expression was also studied, using theoretical analysis and numerical calculation methods. A nonrelativistic spinning gas with an angular velocity  $\omega$  was confined in a long cylinder with radius  $R$  and length  $L$ . In order to simplify the problem and obtain analytical results, the following three assumptions were adopted in the previous theoretical work of ideal gas conducted by Geyko *et al.* [11]: (i) the cylinder is long enough ( $L \gg R$ ), so that end effects are negligible, (ii) the wall of the cylinder is smooth, so that angular momentum is conserved during the compression process; and (iii) compression is a slow and adiabatic process, so that the gas always remains close to equilibrium. All the above assumptions in the previous work have been adopted in this work,

so that it is possible to compare the compression behavior of non-ideal gas and ideal gas under the same condition.

The axial pressure of ideal gas in a cylinder will not be affected by the rotation of the system, as long as the temperature and average density remain the same [11]. Unlike the behavior of ideal gas, it has been found that rotation causes the initial axial pressure of non-ideal gas to be higher than that of the corresponding stationary system. Nevertheless, the axial pressure of the spinning gas will be lower than that of the stationary gas when the compression ratio  $\eta$  is large enough, since the temperature of the spinning gas increase at a slower rate during continuous compression. The behavior of pressure and temperature in gases with different forms of interaction potential energy were compared to illustrate the effect of gas models on gas compression characteristics. The results of this work ratify the conclusion that gas improved compressibility under axial compression.

When verifying the effect of spinning-induced compressibility improvement in real gases, consideration must be given to more complex situations, such as non-equilibrium processes in dynamic compression. Such verification work can be undertaken using numerical simulation methods, such as hydrodynamic simulation [12], discrete lattice Boltzmann methods [13–16], and molecular dynamics methods [17].

In the remainder of this article, a theoretical analysis of the spinning non-ideal gas is presented in Section 2, the numerical results and discussion are in Section 3, and Section 4 presents a short summary of the entire work.

## 2 Theoretical analysis

The EOS of simple gases can be written in the form of a virial expansion [18],

$$p = k_B T(n + Bn^2 + Cn^3 + \dots), \quad (1)$$

in which  $p$  is pressure,  $k_B$  is the Boltzmann constant,  $T$  is temperature,  $n$  is particle number density, and  $B$  and  $C$  are the second and third virial coefficients, respectively. When the density of gas is not very high, the many-body interaction will be far weaker than the pair interaction in the system. Therefore, only the second virial term in the EOS is retained in this work and Eq. (1) can be simplified as,

$$p = k_B T(n + Bn^2). \quad (2)$$

Using isothermal approximation, we have

$$dp = k_B T(1 + 2Bn)dn. \quad (3)$$

The balance between centrifugal force  $dF = n(r)m\omega^2 r dr$  and the pressure difference  $dp$  obtained

$$k_B T(1 + 2Bn)dn = n(r)m\omega^2 r dr. \quad (4)$$

The above equation demonstrates different asymptotic solutions for rare and dense limits. For the rare case ( $2Bn \ll 1$ ), the term  $2Bn$  in Eq. (4) can be ignored, and Eq. (4) becomes the same as the ideal gas equation, whose solution was given by Geyko *et al.* [11] and exhibits an exponential growth with  $r^2$ , as follows:

$$n(r) \rightarrow n_0 \exp\left(\frac{m\omega^2 r^2}{2k_B T}\right), \quad (5)$$

where  $n_0$  is the particle number density at  $r = 0$ . For the dense case ( $2Bn \gg 1$ ), the solution of Eq. (4) tends to

$$n(r) \rightarrow \frac{m\omega^2 r^2}{4Bk_B T} + n_0, \quad (6)$$

indicating a linear growth of  $n(r)$  with  $r^2$ .

In order to simplify the calculation and obtain the key dimensionless parameters of this problem, the dimensionless equation in Eq. (4) can be derived as

$$\left(\frac{1}{\tilde{n}} + \xi\right) d\tilde{n} = 2\varphi \tilde{r} d\tilde{r}, \quad (7)$$

in which

$$\begin{aligned} n_c &= N/V = N/(\pi R^2 L), \quad \tilde{n} = n/n_c, \\ \tilde{r} &= r/R, \quad \xi = 2Bn_c, \quad \varphi = \frac{m\omega^2 R^2}{2k_B T}. \end{aligned} \quad (8)$$

$n_c$  is the critical number density of the system,  $\tilde{n}$  is dimensionless number density,  $\tilde{r}$  is dimensionless radius whose range is  $[0, 1]$ ,  $\xi$  is the dimensionless second virial coefficient and  $\varphi$  correspond to the ratio of spinning kinetic energy at the boundary to the thermal kinetic energy [11]. Integration of Eq. (7) can be written as

$$\ln(\tilde{n}/\tilde{n}_0) + \xi(\tilde{n} - \tilde{n}_0) = \varphi \tilde{r}^2, \quad (9)$$

where  $\tilde{n}_0$  is the dimensionless number density at  $r = 0$  and should be determined using the equation of normalized condition equation:

$$\int_0^1 2\tilde{n}(\tilde{r})\tilde{r}d\tilde{r} = 1. \quad (10)$$

The analytical solution of  $\tilde{n}(\tilde{r})$  can be expressed as

$$\tilde{n}(\tilde{r}) = \frac{1}{\xi} W[\xi \tilde{n}_0 \exp(\varphi \tilde{r}^2 + \xi \tilde{n}_0)], \quad (11)$$

where  $W(x)$  is called the Lambert W function [19] or the product log function, which is the inverse function of  $f(w) = w \cdot \exp(w)$ . The distribution of  $\tilde{n}(\tilde{r})$  can be solved numerically by combining the simultaneous equations in Eq. (9) and Eq. (10). The non-uniform distribution of the number density will result in a non-uniform distribution of pressure, according to Eq. (2), and the average pressure

on the two end faces of the cylinder (hereinafter referred to as “axial pressure”) can be expressed as follows:

$$\begin{aligned} \bar{p} &= \frac{\int_0^R k_B T(n + Bn^2)2\pi r dr}{\int_0^R 2\pi r dr} \\ &= n_c k_B T \int_0^1 (\tilde{n} + \xi \tilde{n}^2) 2\tilde{r} d\tilde{r}. \end{aligned} \tag{12}$$

Now we consider a small axial compression of the system, which causes the length of the cylinder to change from  $L$  to  $L' = L - dL$ . The change in  $L$  will result in a corresponding change in  $\xi$  and  $\varphi$ , and the new value of  $\xi$  after compression can be obtained directly from Eq. (8) and written as

$$\xi' = 2B'n'_c = 2B'n_c \frac{L}{L'}, \tag{13}$$

in which,  $B'$  and  $n'_c = N/(\pi R^2 L')$  are the new values of the second virial coefficient and average number density, respectively, after small compression. The determined value of  $B'$  depends on the temperature after compression and the model of interaction between gas molecules, which is discussed in the following section.

The determination of new  $\varphi$  after compression is much more complicated, because the change in  $\varphi$  will be affected by both  $T$  and  $\omega$ , while the change in  $T$  and  $\omega$  should satisfy the conservation laws of angular momentum and energy during axial compression.

The total angular momentum of the system can be written as

$$\begin{aligned} M &= mL \int_0^R 2\pi r dr n(r) \omega r^2 \\ &= 2\pi m L R^4 \omega n_c \int_0^1 \tilde{n}(\tilde{r}) \tilde{r}^3 d\tilde{r} \\ &= 2m R^2 \omega N \int_0^1 \tilde{n}(\tilde{r}) \tilde{r}^3 d\tilde{r} \end{aligned} \tag{14}$$

and the conservation of angular momentum ( $M = M'$ ) can be written as

$$2m R^2 \omega N \int_0^1 \tilde{n}(\tilde{r}) \tilde{r}^3 d\tilde{r} = 2m R^2 \omega' N \int_0^1 \tilde{n}'(\tilde{r}) \tilde{r}^3 d\tilde{r}, \tag{15}$$

where  $\omega'$  and  $\tilde{n}'$  are the angular speed and dimensionless number density distribution after compression, respectively.

Before giving the energy conservation equation during compression, discussing the relationship between the total energy  $E$  and the system’s state parameters is necessary. For an ideal gas, the internal energy  $U$  is only related to temperature  $T$ , so the total energy can be written as  $E = c_v NT + M\omega/2$ , where  $c_v$  is the specific heat, the first term ( $c_v NT$ ) corresponds to the internal energy, and the second term ( $E_r = M\omega/2$ ) corresponds to the rotational

kinetic energy. However, for non-ideal gases, the internal energy of the system includes not only the kinetic energy of the thermal motion of the molecule  $E_t$  but also the potential energy of the interaction between the molecule’s  $E_p$ .

Directly giving an analytical expression of  $E_p$  for non-ideal gas using the thermodynamic parameters of the system is difficult because only the relationship between  $p$  and the thermodynamic state quantities ( $n$  and  $T$ ) are known. For adiabatic processes only ( $TdS = 0$ ),  $dU = -pdV$  can be obtained, and the change in internal energy and pressure can be directly related to the equation  $p = -(\partial U/\partial V)_S$ . During the compression of spinning gas, although the total heat of the gas in the cylinder  $dQ = 0$ , heat conduction between different parts of the gas occurs due to the non-uniform distribution of  $n(r)$ , which makes the adiabatic conditions fail in the spinning system.

Modeling the form of  $E_p$  to continue the calculation is necessary. The simplest choice for potential energy models is to ignore  $E_p$  ( $E_p = 0$ ), so that the internal energy of non-ideal gas exhibits the same form as the ideal gas. Considering that this model is too simplistic to reflect the influence of  $E_p$  on the compression process, we propose that the potential energy density of the system is equal to the virial pressure  $p_v$ , as  $p_v$  exhibits the same energy density dimension. Pressure can be divided into two parts:  $p_t$  and  $p_v$ , where  $p_t = nk_B T$  is contributed by the thermal motion of the particles, and  $p_v$  is contributed by the interaction between the particles, which can be obtained by  $p_v = p - p_t$ . From this point on, the model of  $dE_p = p_v dV$  is qualitatively reasonable.

The conservation of energy during compression can be expressed as  $pdV = dE$ , where the  $pdV$  work can be approximated by a trapezoidal integral as  $pdV \approx (\bar{p} + \bar{p}')(V - V')/2$  when compression is small, and  $dE$  corresponds to the change of energy during compression. Substituting specific expressions for each part, the expression of total energy is

$$\begin{aligned} E &= E_t + E_p + E_r \\ &= 3Nk_B T/2 + \bar{p}_v V + M\omega/2, \end{aligned} \tag{16}$$

and the conservation of energy can be rewritten as

$$\begin{aligned} (\bar{p} + \bar{p}')(V - V')/2 &= 3Nk_B(T' - T)/2 + (\bar{p}'_v V' - \bar{p}_v V) \\ &\quad + (M'\omega'/2 - M\omega/2). \end{aligned} \tag{17}$$

Solving the simultaneous equations of Eqs. (15) and (17) using an iterative algorithm, the new value of  $\omega'$  and  $T'$  after compression can be determined. Meanwhile, the distribution of density and pressure can be obtained.

Since a continuous compression process with a large compression ratio  $\eta$  can be decomposed into a series of small compression processes, the variation of each physical quantity during a continuous compression can be obtained through the cyclic calculation of the small compression process.

### 3 Numerical results and discussion

#### 3.1 Compression with constant $B$

Strictly speaking, the second virial coefficient  $B$  is a function of temperature  $B(T)$  and will change with a change in  $T$  during compression. Here, for simplicity, we assume that  $B$  is a constant. The effect of temperature on  $B$  will be discussed in the following subsection.

The first significant difference between a spinning non-ideal gas and a spinning ideal gas is that the initial axial pressure in a non-ideal gas is affected by the density distribution. For an ideal gas, when temperature is uniform and determined, the average pressure  $\bar{p} = \bar{n}k_B T$  is only related to the average density and not to the density distribution in the  $r$  direction, as described in previous work [11]. However, for a non-ideal gas, the virial part of the pressure  $p_v$  is proportional to  $n^2$ , and the non-uniform distribution of  $n(r)$  in the rotating system will result in a larger average pressure as the second term in Eq. (12) if  $B$  is positive. That is to say, for virial gas under the same temperature and average density, a larger pressure is required to compress the spinning gas than to compress the static gas, and the spinning gas appears to be more difficult to compress when the compression is not started.

Here, the ratio of  $\bar{p}_r$  to  $\bar{p}_s$  is used to indicate the increase in pressure caused by rotation, in which  $\bar{p}_r$  and  $\bar{p}_s$  are the average axial pressure in the spinning and static system, respectively. The relationship between the pressure ratio  $\bar{p}_r/\bar{p}_s$  and the two dimensionless parameters  $\xi$  and  $\varphi$  are shown in Fig. 1. It is found that, when  $\xi$  is constant, the value of  $\bar{p}_r/\bar{p}_s$  increases as  $\varphi$  increases, indicating that a faster rotation leads to a greater pressure difference. This phenomenon can be explained by the fact that faster rotation results in a greater inhomogeneity of density distribution, which could be derived from Eq. (11).

Meanwhile, the curve of the pressure ratio is not monotonous as  $\xi$  increases when  $\varphi$  is constant. It should be noted that there are two preconditions for the existence of

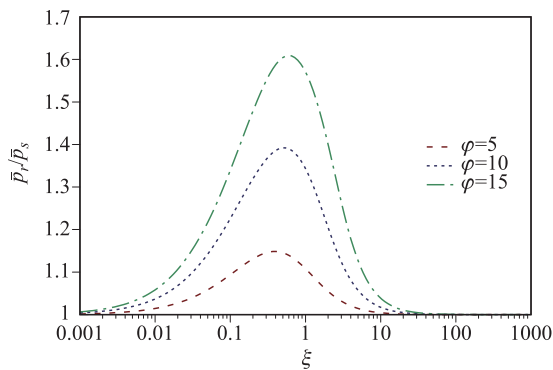


**Fig. 1** The pressure ratio between spinning and static virial gas systems for different  $\xi$  and  $\varphi$  and with the same  $n_c$  and  $T$ .

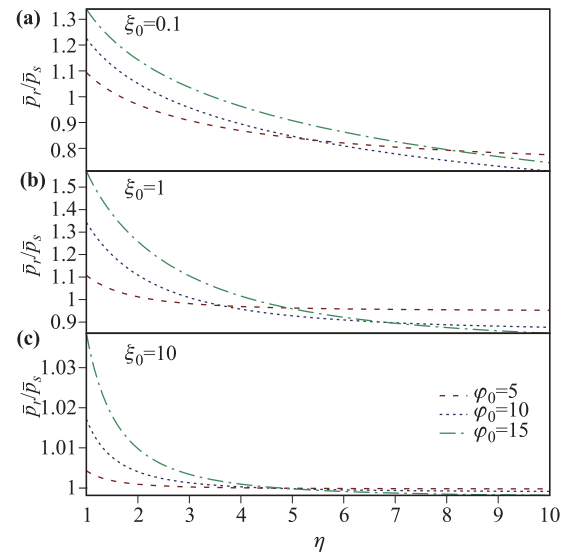


**Fig. 2** Variation of pressure ratio of  $\bar{p}_r$  to  $\bar{p}_s$  during an adiabatic compression for a virial gas system with different initial  $\xi$  and  $\varphi$ . The compression ratio is  $\eta = n_c/n_{c0}$ .

pressure difference between spinning and static systems, one is the virial term in the pressure formula, and the other is the inhomogeneity of density distribution caused by rotation. The proportion of  $p_v$  in the total pressure will increase as  $\xi$  increases, which causes an increase in  $\bar{p}_r/\bar{p}_s$ . Although the density distribution non-uniformity will decrease with an increase of  $\xi$ , the same density difference leads to a greater pressure difference in the case when  $\xi$  is larger, which in turn reduces the value of  $\bar{p}_r/\bar{p}_s$ . Under these two competing mechanisms, the  $\bar{p}_r/\bar{p}_s$  curve reaches its maximum value when  $\xi$  is moderate.

Next, we study the differences in the pressure behavior of the spinning system and the static system during continuous compression. The change in pressure ratio  $\bar{p}_r/\bar{p}_s$  with compression ratio  $\eta$  is illustrated in Fig. 2. When initial  $\xi_0$  is the same, it is found that  $\bar{p}_r/\bar{p}_s$  monotonically decreases with increasing  $\eta$  and is less than one when  $\eta$  is larger than a certain value, indicating that the axial pressure of spinning gas is lower and that spinning gas exhibits an improved compressibility in the latter stages of continuous compression. In addition, it has been found that the effect of compressibility improvement caused by rotation gradually decreases as  $\xi$  increases.

The main reason that  $\bar{p}_r$  in spinning gas increases at a slower rate than  $\bar{p}_s$  in static gas during the compression process is that part of the external  $p dV$  work can be stored in the rotational energy  $E_r$  in the spinning system, making the temperature rise at a slower rate, as illustrated in Fig. 3. It can also be seen in Fig. 3 that the rise in temperature during compression is reduced as  $\xi$  increases. This result could be explained by the fact that a larger  $\xi$  means that the proportion of total energy that is potential energy is greater, and a larger part of the external  $p dV$  work is converted to  $E_p$  during compression.

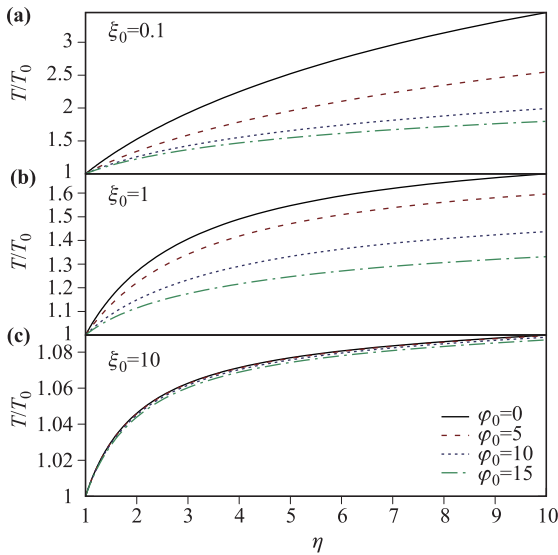


**Fig. 3** Variations in the temperature ratio of  $T$  to  $T_0$  during an adiabatic compression for virial gas system with different initial  $\xi$  and  $\varphi$ .  $T_0$  is the initial temperature.

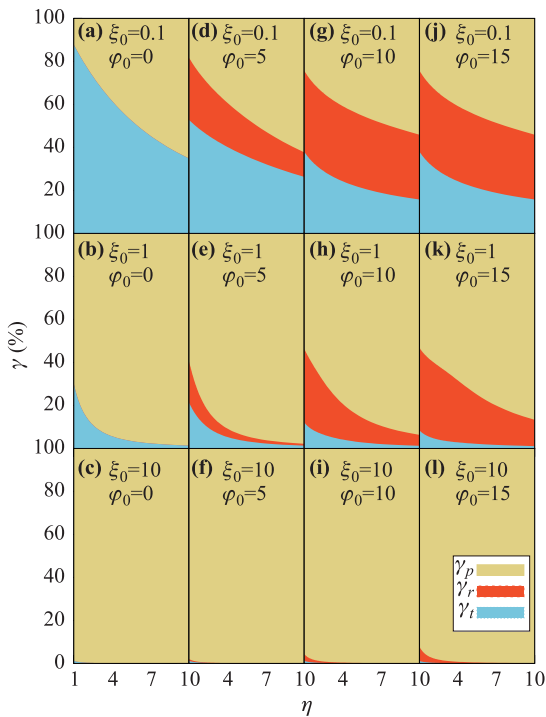


**Fig. 4** The percentage of pdV work converted into thermal ( $\gamma_t$ ), rotational kinetic ( $\gamma_r$ ), and potential ( $\gamma_p$ ) energy during compression, represented by blue, red and yellow, respectively.

The percentage of external pdV work converted to thermal, rotational kinetic, and potential energy during continuous compression, which were presented as  $\gamma_t$ ,  $\gamma_r$ , and  $\gamma_p$ , respectively, are illustrated in Fig. 4 with a different initial  $\xi_0$  and  $\varphi_0$ .

When  $\xi_0$  is the same, it was found that  $\gamma_t$  and  $\gamma_p$  decrease as  $\varphi_0$  increases. While  $\gamma_r$  increases as  $\varphi_0$  increases.

Meanwhile, when  $\varphi_0$  is the same,  $\gamma_p$  increases as  $\xi_0$  increases, indicating that  $\gamma_p$  is positively related to the proportion of potential energy in the system energy. When the interaction of gas molecules is dominant (taking the example of a case with  $\xi_0 = 10$ ), almost all of the pdV work is converted to potential energy, which explains why the temperature rise is so small, as illustrated in Fig. 3(c). Besides, both  $\gamma_t$  and  $\gamma_r$  decrease with an increase in the compression ratio during the compression process, as the value of  $\xi$  increases when  $\eta$  increases.

### 3.2 The effect of $B(T)$

According to the relevant theory of statistical physics [18], the second virial coefficient  $B$  can be written as

$$B(T) = \frac{1}{2} \int (1 - e^{-U_{12}/k_B T}) dV, \quad (18)$$

where  $U_{12}$  is the potential energy of the pair interaction. Therefore,  $B$  is not only a function of temperature, but it is also related to the form of the pair interaction in the system. Assuming that the pair interaction potential between gas molecules exhibits the form of  $U_{12} = \alpha/r^m$  ( $m > 3$ ), the analytical form of  $B(T)$  can be expressed as [18]

$$B(T) = \frac{2\pi}{3} \left( \frac{\alpha}{k_B T} \right)^{3/m} \Gamma \left( 1 - \frac{3}{m} \right), \quad (19)$$

where  $\Gamma(x) = \int_0^\infty t^{x-1} e^{-t} dt$  is the Gamma function. It has been found that  $B(T)$  is inversely proportional to the  $3/m$  power of  $T$ , indicating that high temperatures will weaken the contribution of pair interactions between gas molecules to the virial component of pressure. The previously considered case, where  $B$  is constant, could be regarded as a case whose value of  $m$  tends to infinity.

The axial pressure ratio  $\bar{p}_r/\bar{p}_s$  curves, during an adiabatic compression with different  $\xi_0$  and a different form of  $B(T)$  are plotted in Fig. 5. The value of  $B$  is proportional to  $1/T$  when  $m = 3$  and the correlation between  $B$  and  $T$  weakens as  $m$  increases. Under the same initial conditions ( $\varphi_0$ ,  $\xi_0$ , and  $B_0$ ), the comparison of the axial pressure ratio curves with different forms of  $B(T)$  shows that  $\bar{p}_r/\bar{p}_s$  will increase as  $m$  increases, indicating that the spin-induced compressibility improvement effect is more significant for gases with a larger  $m$ .

It should be noted that this does not mean that the smaller  $m$  is, the more difficult it is for the system to be compressed. The actual situation is just the opposite. If the temperature changes  $\Delta T$  during the compression process are the same, the value of  $B$  in the gas with a smaller  $m$  will be less than that in the gas with a larger  $m$ , thereby making it easier for the gas to be compressed.

The suppression effect of  $B(T)$  on pressure works in both spinning and stationary gases. According to the previous calculation results, it is known that  $\Delta T$  in the stationary system during the compression process is larger

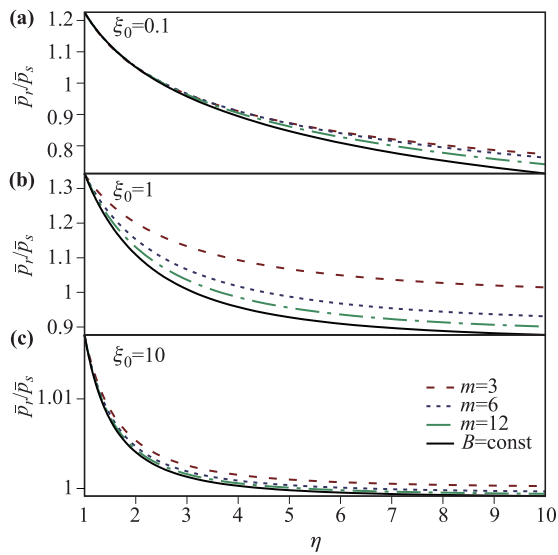


**Fig. 5** Variation in pressure ratio  $\bar{p}_r/\bar{p}_s$  during an adiabatic compression.  $\eta = n_c/n_{c0}$  is the compression ratio. Cases with different initial  $\xi_0$  and  $m$  are plotted in one subfigure to show the effect of  $B(T)$  form on the change in pressure. The initial  $\varphi_0 = 10$  for all curves in this figure.

than that in the spinning system. Therefore, the suppression effect of  $B(T)$  on the pressure during compression is more obvious in the stationary system, resulting in a smaller  $\bar{p}_s$  and a larger pressure ratio  $\bar{p}_r/\bar{p}_s$  in the gas with smaller  $m$ .

The effects of  $B(T)$  on the variation in temperature during compression are illustrated in Fig. 6. It has been found that the temperature ratio  $T_r/T_s$  decreases monotonously as  $\eta$  increases in all cases, indicating that the temperature rise in spinning gas is slower than that in stationary gas. In addition,  $T_r/T_s$  for gas with smaller  $m$  is less than that for gas with larger  $m$ , indicating that the suppression effect of  $B(T)$  on the temperature increase is more significant when  $m$  is smaller.

## 4 Summary

The compressive features of spinning non-ideal gas were investigated using theoretical analysis and numerical calculations. The interaction between the gas molecules causes the spinning gas and the stationary gas to exhibit different initial pressures at the same initial temperature. The analysis of non-ideal gases with various initial parameters in this study shows that, even if the initial pressure of the spinning gas is larger than that of the stationary gas, the temperature rise of the spinning gas is smaller than that of the stationary gas during a continuous quasi-static adiabatic axial compression. This ensures that, when the compression ratio is greater than a certain value, the pressure of the spinning gas is lower than that of stationary gas. The findings of this study verify the robustness of the

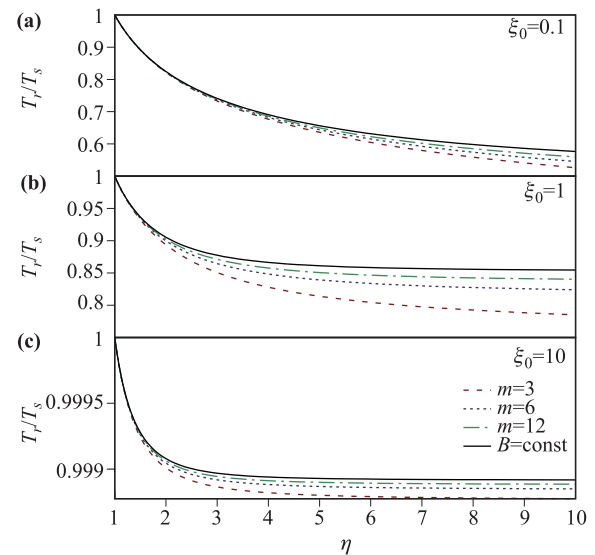


**Fig. 6** The variation in the temperature ratio  $T_r/T_s$  during an adiabatic compression, in which  $T_r$  and  $T_s$  are the temperature in the spinning and stationary system, respectively. Cases with different initial  $\xi_0$  and  $m$  are plotted in one subfigure to show the effect of the form of  $B(T)$  on the variation in temperature. The initial  $\varphi_0 = 10$  for all curves in this figure.

spin-induced compressibility improvement effect in non-ideal gas. In addition, the effects of  $B(T)$  on pressure and temperature during compression were investigated.

The compression ratio considered in this work is based on the average density in the cylinder. For spinning gas, compression caused by centrifugal force along the radial direction is also present, so the highest density in the spinning gas is much larger than the average density  $n_c$ . The corresponding physical picture is that a high-density shell structure is formed near the cylindrical surface. Compared with a uniform system, this shell structure exhibits a larger area density  $\rho R$ , and the increase in  $\rho R$  may correspond to a stronger particle stopping power. The high areal density is a key condition for inertial confinement fusion to achieve ignition. In addition, the device of the Z-pinch experiment is also cylindrical, and one of its goals is to compress high-temperature plasma to an extremely high density and areal density. The compressive feature of spinning gas may exhibits potential value for the design of the Z-pinch scheme.

**Acknowledgements** This work was financially supported by the National Natural Science Foundation of China (Grant No. 11805061), the Natural Science Foundation of Hunan Province, China (Grant No. 2019JJ50072), the Science Challenge Project (Grant No. TZ2016005), and the Fundamental Research Funds for the Central Universities.

## References

1. Z. Fan, Y. Liu, B. Liu, C. Yu, K. Lan, and J. Liu, Non-

- equilibrium between ions and electrons inside hot spots from National Ignition Facility experiments, *Matter and Radiation at Extremes* 2(1), 3 (2017) (I)
2. E. M. Campbell, V. N. Goncharov, T. C. Sangster, S. P. Regan, P. B. Radha, R. Betti, J. F. Myatt, D. H. Froula, M. J. Rosenberg, I. V. Igumenshchev, W. Seka, A. A. Solodov, A. V. Maximov, J. A. Marozas, T. J. B. Collins, D. Turnbull, F. J. Marshall, A. Shvydky, J. P. Knauer, R. L. McCrory, A. B. Sefkow, M. Hohenberger, P. A. Michel, T. Chapman, L. Masse, C. Goyon, S. Ross, J. W. Bates, M. Karasik, J. Oh, J. Weaver, A. J. Schmitt, K. Obenschain, S. P. Obenschain, S. Reyes, and B. Van Wonterghem, Laser-direct-drive program: Promise, challenge, and path forward, *Matter and Radiation at Extremes* 2(2), 37 (2017)
  3. B. Y. Sharkov, D. H. Hoffmann, A. A. Golubev, and Y. Zhao, High energy density physics with intense ion beams, *Matter and Radiation at Extremes* 1(1), 28 (2016)
  4. D. Kraus, J. Vorberger, A. Pak, N. J. Hartley, L. B. Fletcher, S. Frydrych, E. Galtier, E. J. Gamboa, D. O. Gericke, S. H. Glenzer, E. Granados, M. J. MacDonald, A. J. MacKinnon, E. E. McBride, I. Nam, P. Neumayer, M. Roth, A. M. Saunders, A. K. Schuster, P. Sun, T. van Driel, T. Döppner, and R. W. Falcone, Formation of diamonds in laser-compressed hydrocarbons at planetary interior conditions, *Nature Astronomy* 1(9), 606 (2017)
  5. S. V. Lebedev, I. H. Mitchell, R. Aliaga-Rossel, S. N. Bland, J. P. Chittenden, A. E. Dangor, and M. G. Haines, Azimuthal structure and global instability in the implosion phase of wire array Z-pinch experiments, *Phys. Rev. Lett.* 81(19), 4152 (1998)
  6. A. J. Harvey-Thompson, S. V. Lebedev, G. Burdiak, E. M. Waisman, G. N. Hall, F. Suzuki-Vidal, S. N. Bland, J. P. Chittenden, P. De Grouchy, E. Khoory, L. Pickworth, J. Skidmore, and G. Swadling, Suppression of the ablation phase in wire array Z pinches using a tailored current prepulse, *Phys. Rev. Lett.* 106(20), 205002 (2011)
  7. R. P. Drake, High-energy-density physics: Fundamentals, Inertial Fusion, and Experimental Astrophysics, Springer Science & Business Media, 2006
  8. B. L. Holian, Atomistic computer simulations of shock waves, *Shock Waves* 5(3), 149 (1995)
  9. H. Liu, W. Kang, Q. Zhang, Y. Zhang, H. Duan, and X. T. He, Molecular dynamics simulations of microscopic structure of ultra strong shock waves in dense helium, *Front. Phys.* 11(6), 115206 (2016)
  10. H. Liu, Y. Zhang, W. Kang, P. Zhang, H. Duan, and X. T. He, Molecular dynamics simulation of strong shock waves propagating in dense deuterium, taking into consideration effects of excited electrons, *Phys. Rev. E* 95(2), 023201 (2017)
  11. V. I. Geyko and N. J. Fisch, Reduced compressibility and an inverse problem for a spinning gas, *Phys. Rev. Lett.* 110(15), 150604 (2013)
  12. J. Wang, Y. Shi, L. P. Wang, Z. Xiao, X. He, and S. Chen, Scaling and statistics in three-dimensional compressible turbulence, *Phys. Rev. Lett.* 108(21), 214505 (2012)
  13. A. G. Xu, G. C. Zhang, Y. B. Gan, F. Chen, and X. J. Yu, Lattice Boltzmann modeling and simulation of compressible flows, *Front. Phys.* 7(5), 582 (2012)
  14. A. G. Xu, G. C. Zhang, Y. D. Zhang, P. Wang, and Y. J. Ying, Discrete Boltzmann model for implosion- and explosion-related compressible flow with spherical symmetry, *Front. Phys.* 13(5), 135102 (2018)
  15. Y. Gan, A. Xu, G. Zhang, Y. Zhang, and S. Succi, Discrete Boltzmann trans-scale modeling of high-speed compressible flows, *Phys. Rev. E* 97(5), 053312 (2018)
  16. Y. B. Gan, A. G. Xu, G. C. Zhang, C. D. Lin, H. L. Lai, and Z. P. Liu, Nonequilibrium and morphological characterizations of Kelvin-Helmholtz instability in compressible flows, *Front. Phys.* 14(4), 43602 (2019)
  17. S. Plimpton, Fast parallel algorithms for short-range molecular dynamics, *J. Comput. Phys.* 117(1), 1 (1995)
  18. L. D. Landau and E. M. Lifshitz, Course of theoretical physics, Vol. 5, Statistical Physics, Elsevier, 2013
  19. R. M. Corless, G. H. Gonnet, D. E. G. Hare, D. J. Jeffrey, and D. E. Knuth, On the Lambert W-function, *Adv. Comput. Math.* 5(1), 329 (1996)